

# Active Disturbance Rejection Control of Euler-Lagrange Systems Exploiting Internal Damping

Chao Ren, *Member, IEEE*, Yutong Ding, Liang Hu, *Member, IEEE*, Jinguo Liu, *Senior Member, IEEE*, Zhaojie Ju, *Senior Member, IEEE*, and Shugen Ma, *Fellow, IEEE*

**Abstract**—Active disturbance rejection control (ADRC) is an efficient control technique to accommodate both internal uncertainties and external disturbances. In the typical ADRC framework, however, the design philosophy is to “force” the system dynamics into double integral form by extended state observer (ESO) and then controller is designed. Specially, the systems’ physical structure has been neglected in such design paradigm. In this paper, a new ADRC framework is proposed by incorporating at a fundamental level the physical structure of Euler-Lagrange (EL) systems. In particular, the differential feedback gain can be selected considerably small or even zero, due to an effective exploitation of the system’s internal damping. The design principle stems from analysis of the energy balance of EL systems, yielding a physically interpretable design. Moreover, the exploitation of system’s internal damping is thoroughly discussed, which is of practical significance for applications of the proposed design. Besides, a sliding mode ESO is designed to improve the estimation performance over traditional linear ESO. Finally, the proposed control framework is illustrated through tracking control of an omnidirectional mobile robot. Extensive experimental tests are conducted to verify the proposed design as well as the discussions.

## I. INTRODUCTION

Active disturbance rejection control (ADRC) proposed by Han [1] is a well-known approach to cope with dynamic uncertainties and external disturbances of the controlled systems. The key idea is that, the total disturbance (including internal uncertain dynamics, cross couplings and external disturbances) can be on-line estimated by an extended state observer (ESO) and then compensated in the control signal. ADRC has been

This work was supported in part by Tianjin Natural Science Foundation under Grant 18JCQNJC04600, and in part by the National Natural Science Foundation of China under Grant 61603270 (*Corresponding author: Shugen Ma*).

Chao Ren, Yutong Ding and Shugen Ma are with the School of Electrical and Information Engineering, Tianjin University, Tianjin 300072, China (e-mail: renchao@tju.edu.cn; yutong\_ding@tju.edu.cn; shugen.ma@ieee.org).

Liang Hu is with School of Computer Science and Electronic Engineering, University of Essex, UK (e-mail: l.hu@essex.ac.uk).

Jinguo Liu is with State Key Laboratory of Robotics, Shenyang Institute of Automation, Chinese Academy of Sciences, Shenyang 110016, China (e-mail: liujinguo@sia.cn).

Zhaojie Ju is with School of Computing, University of Portsmouth, Portsmouth PO1 3HE, UK (e-mail: zhaojie.ju@port.ac.uk).

Shugen Ma is also with Department of Robotics, Ritsumeikan University, Shiga 525-8577, Japan.

extensively applied to many areas, e.g., robot or vehicle control [2]–[6], networked system control [7]–[10], motor control [11], [12], game strategy synthesis [13]. For more detailed introduction about ADRC, the readers are referred to [14], [15].

In the typical ADRC framework, the design philosophy is reducing system dynamics into the double integral form by linear or nonlinear ESO and then controller is designed (e.g., simple PD controller). Specifically, the control of a complex nonlinear, time-varying and uncertain multi-input multi-output (MIMO) dynamic system is reduced to the simple control problem of double integral plants, by estimating the total disturbance via ESO and compensating it in the control signal. Obviously, this approach greatly simplifies the control system design and has become a general control design framework. It is important to note that, only very partial model information is employed in the typical ADRC framework, while the other known/unknown model information is regarded as the total disturbance. This framework has been widely applied to many practical systems, such as [16]–[25]. However, an important remark here is that the systems’ physical structure has been neglected in this framework. In other words, a physical dynamic system is “forced” into the required double integral form, via “destroying” its structure.

Some works [26]–[29] in the literature incorporate the known model information into ESO and control law, to improve the disturbance estimation performance and control performance. The motivation lies in the fact that the dynamic model is somewhat partially known for many practical dynamic systems. However, these control schemes actually stem from general control system design methodologies, or from mathematical considerations. In other words, the physical structure of dynamic systems is overlooked in the design procedure of these works.

Euler-Lagrange (EL) equations are appropriate to reveal the system’s physical structure [30], such as the workless forces, dissipative forces, etc. In this paper, the term “internal damping” is particularly used to represent the inherent dissipative forces of general EL systems, as opposed to the external damping injected by differential feedback in control. It is related to the Rayleigh dissipation function in the EL equations. The internal damping plays an important role in the energy dissipation of a dynamical system. In the typical ADRC framework, the internal damping is considered as portion of the total disturbance estimated by ESO and is canceled in the control signal. In this way, the resulting double integral

systems do not have any internal damping. Therefore, sufficient external damping has to be injected into the closed-loop system via the differential feedback (i.e., velocity feedback) to guarantee stability of the system. But one problem is that the velocity measurement noises introduced into the control system may deteriorate the control performance.

From the viewpoint of control, the estimated total disturbance in the typical ADRC framework, may contain beneficial components to the control performance, such as the internal damping. In other words, the total disturbance should not be blindly rejected. In this sense, the exploitation of system's internal damping, is equivalent to exploitation of the beneficial components of the estimated total disturbance.

In this paper, a new ADRC framework is proposed by incorporating at a fundamental level the system's physical structure. Specially, the differential feedback gain can be selected considerably small or even zero, due to an effective exploitation of the system's internal damping. Moreover, the proposed ADRC framework is a physically interpretable design, as it is derived from analysis of the system's energy balance. To the best of the authors' knowledge, this is the first work that the system's internal damping is explicitly exploited and discussed in ADRC design.

Firstly, the physical structure of general EL systems is analyzed. More specifically, the generalized forces, i.e., workless forces, internal damping, gravity forces and unknown dynamic forces, are analyzed from the energy dissipation point. Then the design procedure of the proposed ADRC scheme is illustrated by tracking control of an omnidirectional mobile robot (OMR), wherein the robot's internal damping is effectively employed. A sliding mode ESO is proposed to estimate the total disturbance, except the robot's internal damping. More importantly, from the implementation point of view, the exploitation of system's internal damping, is thoroughly discussed and verified by experimental tests.

It is shown in our experimental tests that, the differential feedback gain of the proposed design can be selected considerably small or even zero, while the tracking control performance can be guaranteed. On the contrast, the differential feedback gain of the typical ADRC design should be selected large enough to introduce enough external damping. Meanwhile, severe measurement noises are introduced into the closed-loop system, resulting in strong vibration of the robot and deterioration of the control performance. Besides, in our previous works [31], [32], the internal damping has been exploited in the passivity-based control design for an OMR. The control design objective in [31], [32] is to preserve passivity property of the robot in the closed-loop system, which is completely different with the focus of this paper.

The contributions of this paper are summarized as follows.

1) It is for the first time that the internal damping of EL systems is effectively exploited in the ADRC design. The proposed framework is a physically interpretable design, as the design principle stems from analysis of the system's energy balance. To the best of the authors' knowledge, the system's internal damping has been ignored in previous ADRC works.

2) The exploitation of system's internal damping is thor-

oughly discussed and verified by experimental tests. It is of practical significance for the application of the proposed ADRC framework to general EL systems.

3) A sliding mode ESO is designed to improve the estimation performance of traditional linear ESO. Compared with the traditional linear ESO [33], the designed ESO can achieve superior estimation performances with much lower gains.

The remainder of this paper is organized as follows. In Section II, the physical structure of EL systems and the typical ADRC design are introduced. The proposed ADRC design is presented in Section III. In Section IV, detailed discussions about the exploitation of internal damping are presented. Experimental tests are shown in Section V. Finally, conclusions are drawn in Section VI.

## II. BASICS

### A. Euler-Lagrange (EL) Equations

In this part, the general fully-actuated mechanical systems are taken as an example to show EL equations. Using the Christoffel symbols, the EL equation of general mechanical systems can be written as:

$$\mathbf{M}(\mathbf{q})\ddot{\mathbf{q}} + \mathbf{C}(\mathbf{q}, \dot{\mathbf{q}})\dot{\mathbf{q}} + \frac{\partial \mathbf{F}(\dot{\mathbf{q}})}{\partial \dot{\mathbf{q}}} + \mathbf{g}(\mathbf{q}) + \mathbf{d}(t) = \mathbf{B}(\mathbf{q})\mathbf{u}, \quad (1)$$

where  $\mathbf{q} \in \mathbb{R}^n$  is a set of generalized coordinates for the system;  $\mathbf{M}(\mathbf{q}) \in \mathbb{R}^{n \times n}$  is the inertia matrix;  $\mathbf{C}(\mathbf{q}, \dot{\mathbf{q}}) \in \mathbb{R}^{n \times n}$  is the matrix of Coriolis and centrifugal forces;  $\frac{\partial \mathbf{F}(\dot{\mathbf{q}})}{\partial \dot{\mathbf{q}}}$  is the dissipative forces and  $\mathbf{F}(\dot{\mathbf{q}})$  is the Rayleigh dissipation function;  $\mathbf{g}(\mathbf{q}) \in \mathbb{R}^n$  is the gravity force;  $\mathbf{d}(t) \in \mathbb{R}^n$  represents unknown dynamic forces, including internal uncertainties and external disturbances. The internal uncertainties include parametric uncertainties (unknown system parameters) and non-parametric uncertainties (unmodelled system dynamics) [34], [35];  $\mathbf{B}(\mathbf{q}) \in \mathbb{R}^{n \times n}$  is the control input matrix, and  $\mathbf{u} \in \mathbb{R}^n$  is the control signal. In this paper, the term  $\frac{\partial \mathbf{F}(\dot{\mathbf{q}})}{\partial \dot{\mathbf{q}}}$  is called the internal damping, since it is the inherent dissipative forces of the EL system itself, regardless of external control. To simplify the expression, in the following paper,  $\mathbf{M}$ ,  $\mathbf{C}$ ,  $\mathbf{F}$ ,  $\mathbf{g}$ ,  $\mathbf{d}$  and  $\mathbf{B}$  are used to represent  $\mathbf{M}(\mathbf{q})$ ,  $\mathbf{C}(\mathbf{q}, \dot{\mathbf{q}})$ ,  $\mathbf{F}(\dot{\mathbf{q}})$ ,  $\mathbf{g}(\mathbf{q})$ ,  $\mathbf{d}(t)$  and  $\mathbf{B}(\mathbf{q})$ , respectively.

**Property 1.** In the EL system (1),  $\dot{\mathbf{M}} - 2\mathbf{C}$  is skew-symmetric, i.e.,  $\mathbf{x}^T(\dot{\mathbf{M}} - 2\mathbf{C})\mathbf{x} = 0$ , where  $\mathbf{x} \in \mathbb{R}^n$ .

**Definition** [30]: The system (1) is fully-damped if the Rayleigh dissipation function satisfies:

$$\dot{\mathbf{q}}^T \frac{\partial \mathbf{F}}{\partial \dot{\mathbf{q}}} \dot{\mathbf{q}} \geq \sum_1^n \alpha_i \dot{\mathbf{q}}^2, \quad (2)$$

with  $\alpha_i > 0$  for all  $i \leq n$ . Otherwise, the system (1) is underdamped if  $\exists i \leq n$ , such that  $\alpha_i = 0$ .

In particular, the model (1) can be rewritten in the form of "Newton's second law" as:

$$\underbrace{\mathbf{M}\ddot{\mathbf{q}}}_{\text{mass} \times \text{acceleration}} = \underbrace{\mathbf{B}\mathbf{u} - \mathbf{C}\dot{\mathbf{q}} - \frac{\partial \mathbf{F}}{\partial \dot{\mathbf{q}}} - \mathbf{g} - \mathbf{d}}_{\text{sum of forces}}. \quad (3)$$

The total energy of the system (3) is

$$H_0(\mathbf{q}, \dot{\mathbf{q}}) = \frac{1}{2} \dot{\mathbf{q}}^T \mathbf{M} \dot{\mathbf{q}} + V, \quad (4)$$

where  $V$  is the potential energy function and  $\mathbf{g} \triangleq \frac{\partial V}{\partial \mathbf{q}}$ .

The time derivative of energy function of (4) (i.e., the rate of change of  $H_0(\mathbf{q}, \dot{\mathbf{q}})$ ) is obtained as follows by using Property 1:

$$\begin{aligned} \dot{H}_0 &= \dot{\mathbf{q}}^T \mathbf{M} \ddot{\mathbf{q}} + \frac{1}{2} \dot{\mathbf{q}}^T \dot{\mathbf{M}} \dot{\mathbf{q}} + \mathbf{g}^T \dot{\mathbf{q}} \\ &= \dot{\mathbf{q}}^T (\mathbf{B}\mathbf{u} - \mathbf{C}\dot{\mathbf{q}} - \frac{\partial \mathbf{F}}{\partial \dot{\mathbf{q}}} - \mathbf{g} - \mathbf{d}) + \frac{1}{2} \dot{\mathbf{q}}^T \dot{\mathbf{M}} \dot{\mathbf{q}} + \mathbf{g}^T \dot{\mathbf{q}} \\ &= \dot{\mathbf{q}}^T (\mathbf{B}\mathbf{u} - \frac{\partial \mathbf{F}}{\partial \dot{\mathbf{q}}} - \mathbf{d}). \end{aligned} \quad (5)$$

The integration of the equation above is as follows:

$$\underbrace{H_0(t) - H_0(0)}_{\text{stored energy}} = - \underbrace{\int_0^t \dot{\mathbf{q}}^T \frac{\partial \mathbf{F}}{\partial \dot{\mathbf{q}}} ds}_{\text{dissipated}} + \underbrace{\int_0^t \dot{\mathbf{q}}^T (\mathbf{B}\mathbf{u} - \mathbf{d}) ds}_{\text{supplied}}. \quad (6)$$

As shown in (5) and (6), it is clear that  $\mathbf{C}\dot{\mathbf{q}}$  is workless, since it does not affect the systems' energy balance. Likewise, the gravity force  $\mathbf{g}$  does affect the total energy, yet it does not influence the rate of change of total energy and the energy dissipation. Interestingly, the term  $\mathbf{d}$  does affect the energy balance of the EL systems, however, it cannot be employed, due to the fact that  $\mathbf{d}$  is unknown in practice. It is worth noting that, only the internal damping (i.e.,  $\frac{\partial \mathbf{F}}{\partial \dot{\mathbf{q}}}$ ) influences both the rate of change of the total energy and the dissipated energy of EL systems. As a result, the observations from energy viewpoint provide us control design principles in exploiting the system's physical structure. That is, the internal damping should be effectively employed while the other forces can be rejected, including the workless forces  $\mathbf{C}\dot{\mathbf{q}}$ , gravity forces  $\mathbf{g}$ , and the unknown dynamic forces  $\mathbf{d}$ . In this paper, these forces are regarded as the total disturbance (See Section III).

**Remark 1.** In practical applications, the nominal value of system's internal damping may be time-varying. It can be roughly estimated from the data sheets or simple experiments. Even though the system's internal damping can not be exactly known, it can still be employed in the proposed control framework (see Section IV).

### B. Typical ADRC Design

Considering the general fully-actuated EL system (1), define system's states as  $\mathbf{x}_{01} = \mathbf{q}$  and  $\mathbf{x}_{02} = \dot{\mathbf{q}}$ . The EL system (1) is then transformed into the state space form:

$$\begin{aligned} \dot{\mathbf{x}}_{01} &= \mathbf{x}_{02}, \\ \dot{\mathbf{x}}_{02} &= \mathbf{M}^{-1} \mathbf{B}\mathbf{u} + \underbrace{\mathbf{M}^{-1} [-\mathbf{C}\dot{\mathbf{q}} - \frac{\partial \mathbf{F}}{\partial \dot{\mathbf{q}}} - \mathbf{g} - \mathbf{d}]}_{\mathbf{f}(t)}. \end{aligned} \quad (7)$$

In the typical ADRC framework, the workless forces  $\mathbf{C}\dot{\mathbf{q}}$ , internal damping  $\frac{\partial \mathbf{F}}{\partial \dot{\mathbf{q}}}$ , gravity forces  $\mathbf{g}$  and unknown dynamic forces  $\mathbf{d}$ , are regarded as the total disturbance  $\mathbf{f}(t) \in \mathbb{R}^n$ . It is then viewed as an extended state of the system (7), i.e.,  $\mathbf{x}_{03} = \mathbf{f}(t)$ . The system (7) can be written as:

$$\begin{aligned} \dot{\mathbf{x}}_{01} &= \mathbf{x}_{02} \\ \dot{\mathbf{x}}_{02} &= \mathbf{M}^{-1} \mathbf{B}\mathbf{u} + \mathbf{x}_{03} \\ \dot{\mathbf{x}}_{03} &= \dot{\mathbf{f}}(t) \end{aligned} \quad (8)$$

The typical linear ESO for system (8) can be designed as [33]:

$$\begin{cases} \dot{\mathbf{z}}_{01} = \mathbf{z}_{02} + \beta_{01} \tilde{\mathbf{x}}_{01} \\ \dot{\mathbf{z}}_{02} = \mathbf{z}_{03} + \mathbf{M}^{-1} \mathbf{B}\mathbf{u} + \beta_{02} \tilde{\mathbf{x}}_{01} \\ \dot{\mathbf{z}}_{03} = \beta_{03} \tilde{\mathbf{x}}_{01} \end{cases}, \quad (9)$$

where  $\mathbf{z}_{0i} \in \mathbb{R}^n$  is the estimation of  $\mathbf{x}_{0i}$  ( $i = 1, \dots, n$ );  $\tilde{\mathbf{x}}_{01} = \mathbf{x}_{01} - \mathbf{z}_{01} \in \mathbb{R}^n$ , is the estimation error of state  $\mathbf{x}_{01}$ ; and  $\beta_{0i} \in \mathbb{R}^{n \times n}$  ( $i = 1, 2, 3$ ) are the gain matrices of ESO.

The control law can be designed as:

$$\mathbf{u} = \mathbf{B}^{-1} \mathbf{M}(\mathbf{u}_0 - \mathbf{z}_{03}), \quad (10)$$

where  $\mathbf{u}_0 \in \mathbb{R}^n$  is a new control input to be designed.

With a well-tuned ESO, the state  $\mathbf{z}_{03}$  is able to closely track the total disturbance  $\mathbf{x}_{03} = \mathbf{f}(t)$ . Then the system (8) is reduced into the following decoupled double-integral form by (10):

$$\ddot{\mathbf{q}} \approx \mathbf{u}_0. \quad (11)$$

For the double-integral system above, various control methods can be applied to design  $\mathbf{u}_0$ . The simplest one for  $\mathbf{u}_0$  is PD control:

$$\mathbf{u}_0 = \ddot{\mathbf{q}}_d - \mathbf{K}_p \mathbf{e} - \mathbf{K}_d \dot{\mathbf{e}}, \quad (12)$$

where  $\mathbf{K}_p, \mathbf{K}_d \in \mathbb{R}^{n \times n}$ , are positive diagonal gain matrices;  $\mathbf{q}_d$  is the desired trajectory of  $\mathbf{q}$ ;  $\mathbf{e} = \mathbf{q} - \mathbf{q}_d$ ,  $\dot{\mathbf{e}} = \dot{\mathbf{q}} - \dot{\mathbf{q}}_d$ .

Finally, the control law can be obtained by combining (10) and (12) as:

$$\mathbf{u} = \mathbf{B}^{-1} \mathbf{M}(\ddot{\mathbf{q}}_d - \mathbf{K}_p \mathbf{e} - \mathbf{K}_d \dot{\mathbf{e}} - \mathbf{z}_{03}). \quad (13)$$

It is intuitively clear from (7) that, the internal damping  $\frac{\partial \mathbf{F}}{\partial \dot{\mathbf{q}}}$  is involved in the total disturbance  $\mathbf{f}(t)$ . As  $\mathbf{z}_{03}$  is the estimation of  $\mathbf{f}(t)$  by ESO, it is seen from (10) and (11) that the internal damping has been canceled in the control signal. Attention should be paid to the double-integral form (11) reduced by ESO that it does not have any damping forces. As seen in (12), sufficient external damping (i.e.,  $\mathbf{K}_d \dot{\mathbf{e}}$ ) has to be injected into the closed-loop system via velocity feedback. Thereby, the typical ADRC framework is designed from mathematical considerations, without exploitation of the system's physical structure. In particular, the system's internal damping is completely unemployed.

**Remark 2.** Since system (11) does not have any damping, in order to guarantee the stability, the differential feedback gain  $\mathbf{K}_d$  has to be selected large enough to introduce enough external damping. Severe velocity measurement noises may be also introduced into the control system, as is verified in our experiments.

## III. THE PROPOSED SCHEME

In this part, the proposed ADRC scheme is illustrated by tracking control design for a three-wheeled OMR. Firstly, the robot's dynamic model and its physical structure are briefly introduced. Then the control system is designed with effective exploitation of the robot's internal damping.

TABLE I  
NOMENCLATURE

Parameter	Parameter Definition
<b>World coordinate frame</b>	
$\mathbf{q} = [x \ y \ \theta]^T$	Robot position and orientation angle
<b>Mechanical constants</b>	
$m$	Robot mass
$I_v$	Robot moment of inertia around the mass center of the robot
$I_0$	Combined moment of inertia of motor, gear train and wheel referred to the motor shaft
$L_0$	Contact radius
$r$	Wheel radius
$k_t$	Motor torque constant
$k_b$	Motor back EMF constant
$b_0$	Combined viscous friction coefficient of the motor, gear and wheel shaft
$R_a$	Motor armature resistance
$n$	Gear reduction ratio

### A. Dynamic Model

The robot prototype is shown in Fig. 1 (see Section V), with three Swedish wheels arranged at  $120^\circ$  intervals beneath the steel disk. Each wheel is actuated by a DC motor. It is assumed that no slippage is between the wheel and the motion surface. Only the viscous friction in transmission system is considered. Physical parameters of the OMR are shown in Table I. The robot nominal dynamic model in the world coordinate frame including motor dynamics is given as follows [36]:

$$\mathbf{M}\ddot{\mathbf{q}} + \mathbf{C}\dot{\mathbf{q}} + \mathbf{D}\dot{\mathbf{q}} + \mathbf{d} = \boldsymbol{\tau}, \quad (14)$$

where  $\boldsymbol{\tau} = \mathbf{B}\mathbf{u}$ , and the control input  $\mathbf{u} = [u_1 \ u_2 \ u_3]^T$ , is the supplied voltage of three DC motors; and

$$\mathbf{M} = \frac{1}{p_2} \begin{bmatrix} \frac{3}{2}p_0 + m & 0 & 0 \\ 0 & \frac{3}{2}p_0 + m & 0 \\ 0 & 0 & 3p_0L_0^2 + I_v \end{bmatrix},$$

$$\mathbf{C} = \frac{1}{p_2} \begin{bmatrix} 0 & \frac{3}{2}p_0\dot{\theta} & 0 \\ -\frac{3}{2}p_0\dot{\theta} & 0 & 0 \\ 0 & 0 & 0 \end{bmatrix}, \quad \mathbf{D} = \frac{1}{p_2} \begin{bmatrix} \frac{3}{2}p_1 & 0 & 0 \\ 0 & \frac{3}{2}p_1 & 0 \\ 0 & 0 & 3p_1L_0^2 \end{bmatrix},$$

$$\mathbf{B} = \frac{1}{2} \begin{bmatrix} -\cos\theta - \sqrt{3}\sin\theta & -\cos\theta + \sqrt{3}\sin\theta & 2\cos\theta \\ -\sin\theta + \sqrt{3}\cos\theta & -\sin\theta - \sqrt{3}\cos\theta & 2\sin\theta \\ 2L_0 & 2L_0 & 2L_0 \end{bmatrix},$$

$$p_0 = \frac{n^2 I_0}{r^2}, \quad p_1 = \frac{n^2}{r^2} (b_0 + \frac{k_t k_b}{R_a}), \quad p_2 = \frac{n k_t}{r R_a}.$$

The robot dynamic model (14) is similar to the EL equation (1), except the gravity forces. Notably,  $\mathbf{D}\dot{\mathbf{q}}$  is the robot's internal damping, due to the combined viscous friction of the motor, gear and wheel shaft, as well as the motor armature resistance, etc. By the way, it is obvious that the OMR is fully-damped.

### B. Sliding Mode ESO design

To improve the estimation performance of traditional linear ESO, a sliding mode ESO (SMESO) is designed to estimate the total disturbance. Define state variables as  $\mathbf{x}_1 = \mathbf{q}$ ,  $\mathbf{x}_2 = \dot{\mathbf{q}}$  and the extended total disturbance state as  $\mathbf{x}_3 = \mathbf{f}(t)$ . The robot dynamic model (14) can be written in the state space form with an extended state as:

$$\begin{aligned} \dot{\mathbf{x}}_1 &= \mathbf{x}_2, \\ \dot{\mathbf{x}}_2 &= \mathbf{M}^{-1}\boldsymbol{\tau} - \mathbf{M}^{-1}\mathbf{D}\dot{\mathbf{q}} + \mathbf{x}_3, \\ \dot{\mathbf{x}}_3 &= \dot{\mathbf{f}}(t). \end{aligned} \quad (15)$$

Here,  $\mathbf{f}(t)$  only includes the workless forces  $\mathbf{C}\dot{\mathbf{q}}$ , and unknown dynamic forces  $\mathbf{d}$ , i.e.,  $\mathbf{f}(t) = \mathbf{M}^{-1}(-\mathbf{C}\dot{\mathbf{q}} - \mathbf{d})$ . Note that, the robot's internal damping  $\mathbf{D}\dot{\mathbf{q}}$  is not included in the total disturbance  $\mathbf{f}(t)$ , which is the essential difference with the typical ADRC design (7).

Define  $\mathbf{z}_i$  ( $i = 1, 2, 3$ ) as the estimation of  $\mathbf{x}_i$  ( $i = 1, 2, 3$ ). Consider a sliding manifold as:

$$\mathbf{s} = \dot{\tilde{\mathbf{e}}} + \boldsymbol{\Lambda}\tilde{\mathbf{e}}, \quad (16)$$

where  $\tilde{\mathbf{e}} = \mathbf{q} - \mathbf{z}_1$ ,  $\boldsymbol{\Lambda} \in \mathbb{R}^{3 \times 3}$  is a diagonal positive definite matrix, and  $\mathbf{s} = [s_1 \ s_2 \ s_3]^T$ .

In order to reduce the chattering, the following time-continuous reaching law is employed:

$$\dot{\mathbf{s}} = -k\mathbf{s} - \boldsymbol{\gamma}fal(\mathbf{s}, \alpha, \delta), \quad (17)$$

where  $k > 0$  is a constant,  $\boldsymbol{\gamma} \in \mathbb{R}^{3 \times 3}$  is a diagonal positive definite matrix,

$$fal(\mathbf{s}, \alpha, \delta) = \begin{bmatrix} fal(s_1, \alpha, \delta) & fal(s_2, \alpha, \delta) & fal(s_3, \alpha, \delta) \end{bmatrix}^T,$$

and

$$fal(s_i, \alpha, \delta) = \begin{cases} |s_i|^\alpha sgn(s_i) & |s_i| > \delta \\ \frac{s_i}{\delta^{1-\alpha}} & |s_i| \leq \delta \end{cases}, \quad i = 1, 2, 3,$$

where  $\delta > 0$ , and  $0 < \alpha \leq 1$ ; and

$$sgn(s_i) = \begin{cases} 1, & s_i > 0 \\ 0, & s_i = 0 \\ -1, & s_i < 0 \end{cases}.$$

Then the following SMESO is obtained:

$$\begin{cases} \dot{\mathbf{z}}_1 = \mathbf{z}_2 + k_1\mathbf{s} + \boldsymbol{\gamma}_1fal(\mathbf{s}, \alpha_1, \delta) \\ \dot{\mathbf{z}}_2 = \mathbf{z}_3 - \mathbf{M}^{-1}\mathbf{D}\dot{\mathbf{q}} + \mathbf{M}^{-1}\boldsymbol{\tau} + k_2\mathbf{s} + \boldsymbol{\gamma}_2fal(\mathbf{s}, \alpha_2, \delta), \\ \dot{\mathbf{z}}_3 = k_3\mathbf{s} + \boldsymbol{\gamma}_3fal(\mathbf{s}, \alpha_3, \delta) \end{cases}, \quad (18)$$

where the diagonal positive definite matrices  $\boldsymbol{\gamma}_i$ ,  $i = 1, 2, 3$ , are observer gains, and  $k_i > 0$ .

Compared with linear ESO (9), the SMESO can achieve superior performances with lower gains, such as: 1) higher response speed; 2) much higher estimation accuracy; 3) much smaller phase lag. The simulation verification is not shown in this paper due to page limitations.

Define estimation errors of SMESO as  $\tilde{x}_i = x_i - z_i$ ,  $i = 1, 2, 3$ . The estimation error dynamics is obtained as:

$$\begin{cases} \dot{\tilde{x}}_1 = \tilde{x}_2 - k_1 s - \gamma_1 \text{fal}(s, \alpha_1, \delta) \\ \dot{\tilde{x}}_2 = \tilde{x}_3 - k_2 s - \gamma_2 \text{fal}(s, \alpha_2, \delta) \\ \dot{\tilde{x}}_3 = \dot{f}(t) - k_3 s - \gamma_3 \text{fal}(s, \alpha_3, \delta) \end{cases} \quad (19)$$

**Theorem 1.** Assuming that  $\dot{f}(t)$  is bounded, with the sliding manifold (16), the estimation errors  $\tilde{x}_1$  and  $\tilde{x}_2$  are asymptotically convergent, i.e.,  $\tilde{x}_1, \tilde{x}_2 \rightarrow \mathbf{0}$  as  $t \rightarrow \infty$ . Besides, the bounded convergence of the estimation error  $\tilde{x}_3$  is guaranteed, i.e.,  $|\tilde{x}_{3j}| \leq \sigma_{3j}$  ( $j = 1, 2, 3$ ), where  $\sigma_{3j}$  and  $\tilde{x}_{3j}$  respectively represent the  $j$ th element of  $\sigma_3$  and  $\tilde{x}_3$ . Specially, if  $\dot{f}(t) = \mathbf{0}$ , then  $\tilde{x}_3 \rightarrow \mathbf{0}$  as  $t \rightarrow \infty$ . Then the estimation error dynamics (19) is asymptotically stable.

The proof of *Theorem 1* is given in Appendix.

**Remark 3.** Many methods can improve the estimation performance of ESO. One way is to incorporate the known model information into ESO [37]. In real applications, the nominal value of internal damping can be easily obtained, and can be viewed as partial known model information. In this sense, the exploitation of the system's internal damping is equivalent to incorporating partial known model information into ESO (see (18)). Thereby, the estimation performance of ESO can be improved by exploitation of the system's internal damping.

### C. Controller Design

The control efforts can be divided into two parts. The first part of control efforts is as follows:

$$\tau_1 = -Mz_3. \quad (20)$$

The first part of control efforts is used to compensate the total disturbance estimated by the SMESO, such that the robot dynamic model (14) in practice is approximately reduced to the following form:

$$M\ddot{q} + D\dot{q} = \tau_2. \quad (21)$$

It should be reminded that  $M$  and  $D$  are the nominal values.

The other part of control efforts is designed to achieve trajectory tracking, which effectively exploits the internal damping of OMR. It has:

$$\tau_2 = M(\ddot{q}_d - K_p e - K_d \dot{e}) + D\dot{q}_d, \quad (22)$$

where  $q_d(t) = [x_d \ y_d \ \theta_d]^T$  is the reference trajectory;  $e = q - q_d$ ,  $\dot{e} = \dot{q} - \dot{q}_d$ , and  $K_p, K_d \in \mathbb{R}^{3 \times 3}$ , are positive diagonal gain matrices.

The control efforts are obtained by combining (20) and (22):

$$\tau = \tau_1 + \tau_2 = M(\ddot{q}_d - K_p e - K_d \dot{e} - z_3) + D\dot{q}_d. \quad (23)$$

Note that  $\tau = Bu$ , thus the final control input  $u$  is obtained as follows:

$$u = B^{-1}\tau. \quad (24)$$

Assuming that  $\tilde{x}_3$  is quite small, and combining (14) and (23), error dynamics of the closed-loop system can be obtained as:

$$\ddot{e} + K_{de}\dot{e} + K_p e \approx \mathbf{0}, \quad (25)$$

where  $K_{de} = M^{-1}D + K_d$ , is considered as the equivalent differential feedback gain matrix. Here, it is needed to distinguish between  $M^{-1}D\dot{e}$  and  $D\dot{q}$ .  $M^{-1}D\dot{e}$  is the internal damping preserved in the closed-loop system (25), while  $D\dot{q}$  is the internal damping of the open-loop dynamic system (14).

For the sake of simplicity, all of the poles of the decoupled error dynamics (25) in three channels are placed at the same desired locations. It is given as follows:

$$K_p = \begin{bmatrix} \omega_c^2 & 0 & 0 \\ 0 & \omega_c^2 & 0 \\ 0 & 0 & \omega_c^2 \end{bmatrix}, K_{de} = \begin{bmatrix} 2\xi\omega_c & 0 & 0 \\ 0 & 2\xi\omega_c & 0 \\ 0 & 0 & 2\xi\omega_c \end{bmatrix},$$

where  $\omega_c$  ( $\omega_c > 0$ ) is the bandwidth of the controller [38], and  $\xi > 0$  is a parameter of damping ratio.

Let  $E = [e^T \ \dot{e}^T]^T$ . Then (25) can be written as:

$$\dot{E} = A_e E + A_x \tilde{x}_3, \quad (26)$$

where

$$A_e = \begin{bmatrix} O_3 & I_3 \\ -K_p & -K_{de} \end{bmatrix}, A_x = \begin{bmatrix} O_3 \\ I_3 \end{bmatrix}.$$

**Theorem 2.** Assuming  $\dot{f}(t)$  is bounded,  $\forall \omega_c > 0$ , there exists a positive constant vector  $\rho = [\rho_1 \ \rho_2 \ \dots \ \rho_6]^T$  such that every element  $E_i$  of  $E$  finally satisfies  $|E_i| \leq \rho_i$  ( $i = 1, 2, \dots, 6$ ).

The proof of *Theorem 2* is given in Appendix.

It is noted that the internal damping  $D\dot{q}$  is not canceled in the control signal (24), since it is not included in the estimated disturbance  $z_3$ . By contrast, in the typical ADRC, the internal damping, as portion of the total disturbance (see (7)), has been canceled in the control signal (13). On the other hand, it can be seen from the reduced model (21) that the internal damping is preserved, whereas the reduced model (11) is double integral form without any damping.

**Remark 4.** The energy function of open-loop dynamic system (14) is  $H_0(q, \dot{q}) = \frac{1}{2}\dot{q}^T M \dot{q}$ . The controller (23) actually modifies the energy function  $H_0(q, \dot{q})$  into:  $H(e, \dot{e}) = \frac{1}{2}\dot{e}^T M \dot{e} + \frac{1}{2}e^T M K_p e$ . The time derivative of energy function along the closed-loop system (25) becomes:  $\dot{H}(e, \dot{e}) = -\dot{e}^T (D + M K_d) \dot{e}$ . It is intuitively clear that even though the gain  $K_d$  is set as zero,  $\dot{H}(e, \dot{e}) < 0$  can be guaranteed. In other words, the closed-loop system is still stable due to an effective exploitation of the robot's internal damping, without differential feedback.

**Remark 5.** Particular attention should be paid to the term  $D\dot{q}_d$  in (23). It is interesting that  $D\dot{q}_d$  actually introduces the damping of  $M^{-1}D\dot{e}$  to the closed-loop system (25), yet without using any differential feedback. However, in the typical ADRC design (13), the damping has to be injected via differential feedback  $K_d \dot{e}$ .

## IV. DISCUSSIONS

As presented before, the exploitation of system's internal damping can not only improve the estimation performance of ESO, but also greatly reduce external damping injection in the

controller. However, when applying the proposed scheme in practice, four key aspects should be carefully discussed.

(1) The first key aspect is about the system's inherent characteristic, i.e., whether the internal damping preserved in the closed-loop system (25), i.e.,  $M^{-1}D\dot{e}$ , is sufficient. Therefore, the first step in applying the proposed scheme is to evaluate the internal damping related term  $M^{-1}D$ . If the term  $M^{-1}D$  is small, external damping injection is required via a positive  $K_d$ . If  $M^{-1}D$  is proper, the external damping injection via differential feedback can be avoided, i.e.,  $K_d = 0$ . Actually, it is verified in our experimental tests that the closed-loop system of OMR can achieve superior performance without any external damping injection (see Section V).

If  $M^{-1}D$  is too large, the system's internal damping is excessive. In this case, damping of the closed-loop system (25) can be reduced by properly choosing a certain negative  $K_d$ . Note that  $K_d$  should be carefully set, to guarantee the system stability (i.e.,  $K_{de}$  in (25) should be positive).

Another solution for this case is only to use partial internal damping in ESO and controller. This is because the residual internal damping can be viewed as portion of the total disturbance, and then compensated in the control signal. This solution is suggested in practice, since the negative  $K_d$  is avoided.

(2) The second one is also about the system's inherent feature, i.e., fully damped or underdamped [30]. For both fully damped and underdamped MIMO systems, the internal damping of each channel is usually different. Therefore, the injected external damping is usually different for each channel. In other words, the diagonal elements of the differential gain matrix  $K_d$  in (25) should be set individually for each channel. It differs from the typical ADRC scheme that the external damping injection can be set as the same for each channel. This is because the reduced system of typical ADRC scheme is double integral form for each channel without any damping (see equation (11)).

Specially, for underdamped systems, the gain matrix  $K_d$  in (25) should be carefully set to avoid system instability, as the internal damping is lack in at least one channel. Sufficient external damping should be injected to the channels without internal damping.

(3) The third important aspect arises from parameter uncertainties, i.e., the internal damping related term  $M^{-1}D$  in the closed-loop system may be underestimated or overestimated. It is known that it is difficult to obtain the exact dynamic model. However, the nominal value of  $M$  and  $D$  can be used in the proposed control scheme, no matter it is underestimated or overestimated. This is because,  $M$  and  $D$  in the robot dynamics (14) are reshaped to their nominal value in (21), while the resulting parameter uncertainties are involved in the total disturbance.

For example, if  $M^{-1}D$  is underestimated, it is similar to the case that the internal damping is insufficient. Then external damping injection is required via a positive  $K_d$ . On the contrary, if  $M^{-1}D$  is overestimated, the damping of the closed-loop system can be reduced by properly choosing a certain negative  $K_d$ , or by using only partial internal damping in ESO and controller.

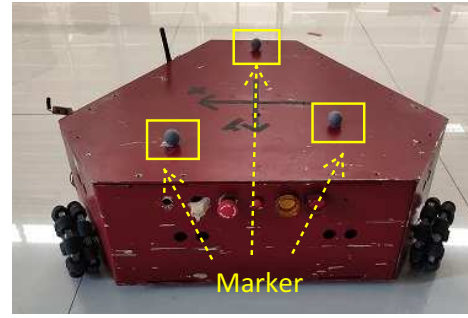


Fig. 1. Robot prototype.

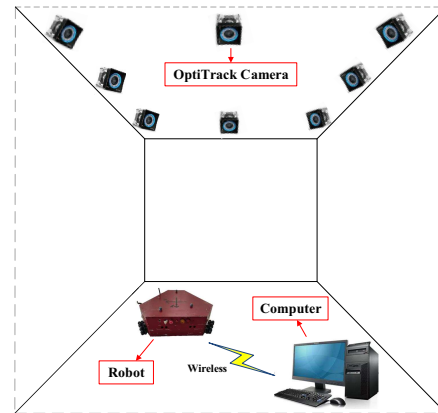


Fig. 2. Experimental setup.

(4) The last one is about the specific parameter setting of  $K_d$ . By detailed analysis above, the gain  $K_d$  in (25) for external damping injection can be determined following the subsequent three steps. That is: 1) estimate the damping inherent in the closed-loop system, i.e.,  $M^{-1}D$ ; 2) select the desired gain  $K_{de} = M^{-1}D + K_d$  in (25); 3) calculate the  $K_d$  as  $K_d = K_{de} - M^{-1}D$ .

## V. EXPERIMENTS

### A. Experimental setup

The robot prototype and experimental setup are respectively shown in Fig. 1 and Fig. 2. The control algorithm was implemented via MATLAB on a personal computer (Intel(R) Core(TM) i7-4770 CPU@3.40GHz). The control signal (motor voltage) generated by the computer was then transmitted to the robot prototype through wireless communication (2.4G WIFI). The robot position was obtained using the OptiTrack motion capture system, which consists of eight capture cameras (part NO. Prime 41) and can realize positioning accuracy within 2 mm. The robot prototype is shown in Fig. 1. The sample time was set as 30 ms.

The robot physical parameters were estimated as follows:  $m = 19.1$  kg,  $I_v = 0.65$  kg · m<sup>2</sup>,  $r = 0.05$  m,  $L_0 = 0.25$  m,  $I_0 = 1.47 \times 10^{-5}$  kg · m<sup>2</sup>,  $b_0 = 1.0 \times 10^{-8}$  Nms/rad,  $k_b = 0.02076$  V · s/rad,  $k_t = 0.0259$  N · m/A,  $R_a = 1.53$  Ω,  $n = 71$ .

The robot was commanded to track a square trajectory, with side length of 1 m and translational velocity of 0.1 m/s. The desired rotational motion is as:

$$\theta_d[\text{rad}] = \begin{cases} 0, & 0s \leq t < 10s \\ \frac{\pi}{10}(t - 10), & 10s \leq t < 20s \\ \pi, & 20s \leq t < 30s \\ \frac{\pi}{10}(t - 30) + \pi, & 30s \leq t \leq 40s \end{cases}$$

## B. Experimental Scenarios

In this part, the typical ADRC scheme in Section II is also tested. For the sake of comparison, control laws of the proposed control approach and typical ADRC are respectively written as follows:

$$\tau = M(\ddot{q}_d - K_p e - K_d \dot{e} - z_3) + D\dot{q}_d, \quad (27a)$$

$$\tau = M(\ddot{q}_d - K_p' e - K_d' \dot{e} - z_3'). \quad (27b)$$

The closed-loop error dynamics of the two control schemes are shown as follows:

$$\ddot{e} + K_{de} \dot{e} + K_p e = \tilde{x}_3, \quad (28a)$$

$$\ddot{e} + K_d' \dot{e} + K_p' e = \tilde{x}_3', \quad (28b)$$

where (28a) and (28b) are the error dynamics of the proposed approach and the typical ADRC, respectively. Note  $K_{de} = M^{-1}D + K_d$ .

According to the physical parameters of OMR, the internal damping related term  $M^{-1}D$  is estimated as:

$$M^{-1}D = \begin{bmatrix} 13.43 & 0 & 0 \\ 0 & 13.43 & 0 \\ 0 & 0 & 17.19 \end{bmatrix}.$$

Three experimental scenarios are presented here.

1) *The first scenario*: In the first experimental scenario, no external damping is injected into either the proposed control scheme or the typical ADRC scheme. In other words, both  $K_d$  and  $K_d'$  were set to zero. In this way, only the internal damping can be employed.

Control parameters of the proposed control (27a) and the typical ADRC (27b) were set as the same:

$$K_p = K_p' = \begin{bmatrix} 9 & 0 & 0 \\ 0 & 9 & 0 \\ 0 & 0 & 9 \end{bmatrix}, \quad K_d = K_d' = \begin{bmatrix} 0 & 0 & 0 \\ 0 & 0 & 0 \\ 0 & 0 & 0 \end{bmatrix}.$$

It is necessary to note that the typical ADRC was not tested in this scenario, since the control system exhibits undamped oscillations. This is due to the fact that the closed-loop system (28b) does not have any internal damping, if  $K_d' = 0$ .

TABLE II  
IAE AND MAE OF THE FIRST SCENARIO.

Index	IAE <sub>xy</sub> (m)	IAE <sub>θ</sub> (rad)	MAE <sub>xy</sub> (m)	MAE <sub>θ</sub> (rad)
Proposed	0.3050	1.0963	0.0210	0.1048

2) *The second scenario*: In the second scenario, the gains for proportional feedback and differential feedback were respectively set the same for both controllers (27a) and (27b), i.e.,  $K_p = K_p'$  and  $K_d = K_d'$ . Therefore, the external damping introduced by differential feedback is identical for both controllers. Also, the differential feedback gains,  $K_d$  and  $K_d'$ , were deliberately set small. In this way, the advantages of exploiting robot's internal damping can be clearly demonstrated.

$$K_p = K_p' = \begin{bmatrix} 9 & 0 & 0 \\ 0 & 9 & 0 \\ 0 & 0 & 9 \end{bmatrix}, \quad K_d = K_d' = \begin{bmatrix} 4.57 & 0 & 0 \\ 0 & 4.57 & 0 \\ 0 & 0 & 0.81 \end{bmatrix}.$$

Note that the parameters above were given by setting  $\omega_c = 3$  rad/s and  $\xi = 3$  (see Section III-C).

3) *The third scenario*: In the third scenario, the differential gain  $K_d'$  of the typical ADRC was increased to introduce enough damping, such that the error dynamics (28a) and (28b) have the same damping. That is  $K_d' = K_{de}$ . The purpose is to compare the measurement noises introduced by both controllers when the two closed-loop systems have similar performance. The control parameters in (28a) and (28b) were set as:

$$K_p = K_p' = \begin{bmatrix} 9 & 0 & 0 \\ 0 & 9 & 0 \\ 0 & 0 & 9 \end{bmatrix}, \quad K_d' = K_{de} = \begin{bmatrix} 18 & 0 & 0 \\ 0 & 18 & 0 \\ 0 & 0 & 18 \end{bmatrix},$$

and  $K_d = K_{de} - M^{-1}D$ .

Besides, the observer parameters of the proposed SMESO were set as:  $\alpha_1 = 1$ ,  $\alpha_2 = 0.5$ ,  $\alpha_3 = 0.25$ ,  $\delta = 10$ ,  $k_1 = 1$ ,  $k_2 = 10$ ,  $k_3 = 100$ ,  $\mathbf{\Lambda} = \text{diag}(1, 1, 1)$ ,  $\gamma_1 = \text{diag}(24, 24, 24)$ ,  $\gamma_2 = \text{diag}(51.2, 51.2, 51.2)$ ,  $\gamma_3 = \text{diag}(57, 57, 57)$ . For the parameter tuning, it can refer to [1], [39].

The typical ESO parameters of ADRC were set as follows:  $\beta_{01} = \text{diag}(24, 24, 24)$ ,  $\beta_{02} = \text{diag}(192, 192, 192)$ ,  $\beta_{03} = \text{diag}(512, 512, 512)$ .

## C. Experimental results

The integral of absolute error (IAE) and maximum absolute error (MAE) were used to evaluate the control performances. The definition of IAE and MAE are as follows:

$$\begin{cases} IAE_{xy}[\text{m}] = \int_0^T (|e_x| + |e_y|) dt \\ IAE_{\theta}[\text{rad}] = \int_0^T |e_{\theta}| dt \\ MAE_{xy}[\text{m}] = \max \left\{ \max |e_x|, \max |e_y| \right\} \\ MAE_{\theta}[\text{rad}] = \max |e_{\theta}| \end{cases}.$$

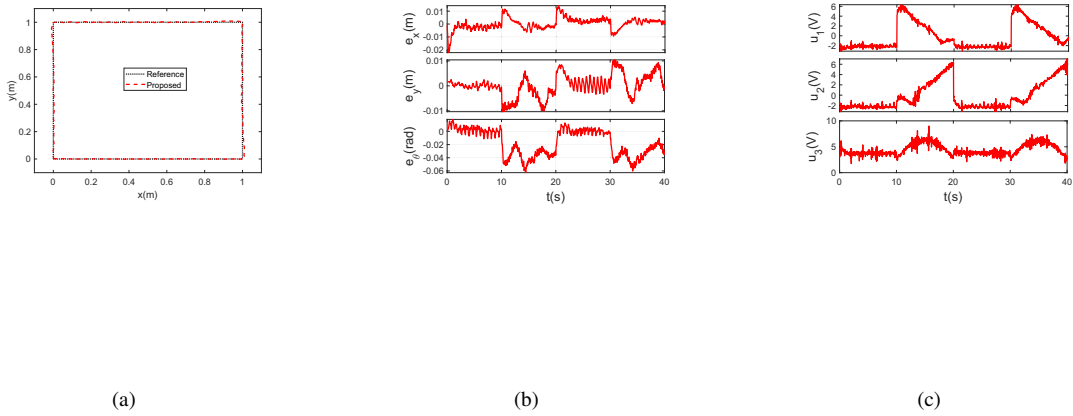


Fig. 3. Experiments results of the first scenario. (a) Reference trajectory and responses in the xy-plane. (b) Tracking errors. (c) Control input  $u(t)$ , i.e., motor voltages.

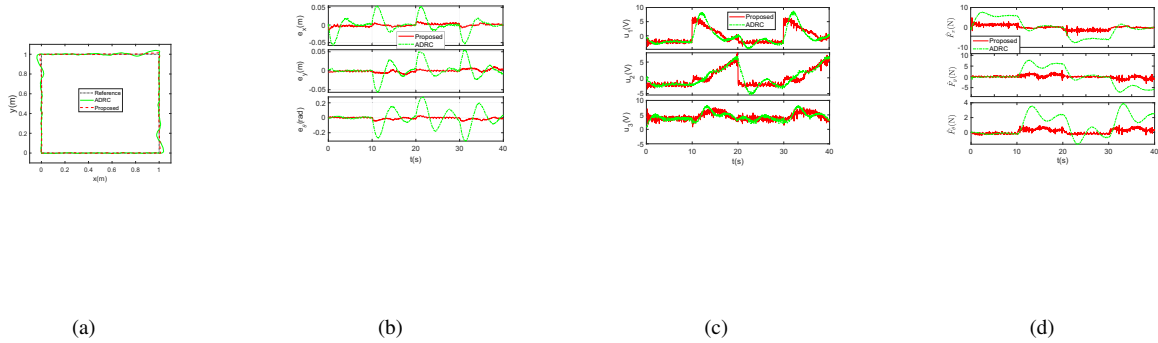


Fig. 4. Experiments results of the second scenario. (a) Reference trajectory and responses in the xy-plane. (b) Comparison of tracking errors. (c) Control input  $u(t)$ , i.e., motor voltages. (d) Estimated disturbances  $f(t)$  by SMESO and typical linear ESO.

TABLE III  
IAE AND MAE OF THE SECOND SCENARIO.

Index	$IAE_{xy}(m)$	$IAE_\theta(rad)$	$MAE_{xy}(m)$	$MAE_\theta(rad)$
ADRC	1.0525	3.3197	0.0519	0.3116
Proposed	0.2382	0.4743	0.0151	0.0469

1) *Results of the first scenario:* Experimental results of the first scenario are shown in Fig. 3. The IAE and MAE are presented in Table II. It is shown in Fig. 3 (a) that the proposed control system achieves the steady-state tracking error within 1 cm and 0.06 rad, while the differential feedback gain was set as  $K_d = 0$ . This confirms that the proposed scheme can achieve superior control performance only using the internal damping, without any external damping injection. It also indicates that the robot has enough internal damping to guarantee the system performance.

2) *Results of the second scenario:* Experimental results of the second scenario are shown in Fig. 4 and Table III. It can be observed from Fig. 4 (a) and (b) that compared with ADRC, the tracking response of the proposed control scheme is eminent, with much smaller overshoot. However, the tracking response of typical ADRC has large overshoot and severe oscillations. Table III illustrates that the  $IAE_{xy}$  and  $IAE_\theta$  of typical ADRC are 4.4 times and 7.0 times as large as those of the proposed control design, respectively.  $MAE_{xy}$  and  $MAE_\theta$  of the typical ADRC are 3.4 times and 6.6 times as large as those of the proposed control design, respectively. Fig. 4 (c) compares the control inputs of the two control approaches. Fig. 4 (d) shows the estimated total disturbance by SMESO and linear ESO, wherein the main difference is that the internal damping is not involved in the total disturbance estimated by SMESO.

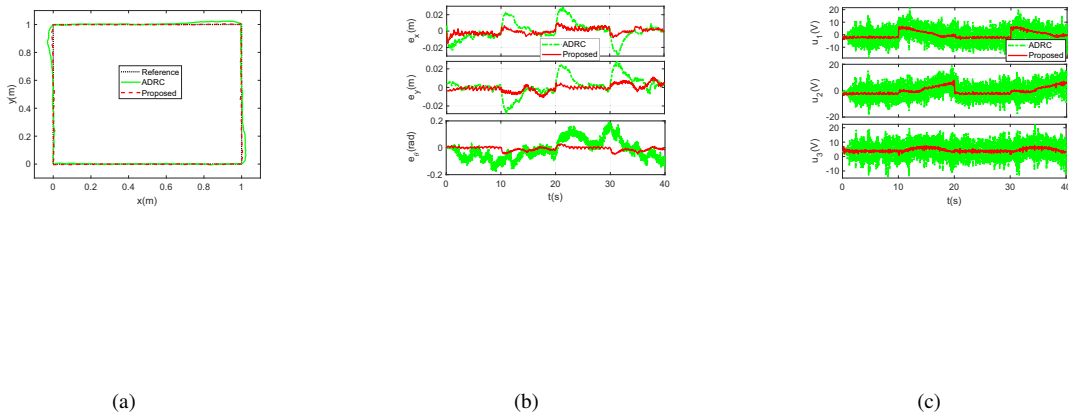


Fig. 5. Experiments results of the third scenario. (a) Reference trajectory and responses in the xy-plane. (b) Tracking errors. (c) Control input  $u(t)$ , i.e., motor voltages.

TABLE IV  
IAE AND MAE OF THE THIRD SCENARIO.

Index	$IAE_{xy}(m)$	$IAE_\theta(rad)$	$MAE_{xy}(m)$	$MAE_\theta(rad)$
ADRC	0.6106	2.5210	0.0306	0.1917
Proposed	0.2382	0.4743	0.0151	0.0469

In this experimental scenario, it is reminded that  $K_d$  and  $K_d'$  were deliberately set the same and small. The damping in the proposed control (28a) is  $(M^{-1}D + K_d)\dot{e}$ , while the damping in typical ADRC (28b) is only  $K_d'\dot{e}$ . Therefore, the internal damping of the robot is preserved in the proposed design. However, the typical ADRC does not employ any internal damping. As a result, if small external damping is injected, the typical ADRC does not have enough damping and the control performance is deteriorated. The experimental results are in good agreement with the theoretical analysis.

3) *Results of the third scenario:* Experimental results of the third scenario are shown in Fig. 5. As shown in Fig. 5 (c), much more measurement noises are introduced into the control signals of typical ADRC, even though both closed-loop systems (28a) and (28b) have the same proportional gain and equivalent differential gain (i.e.,  $K_d' = K_{de}$  and  $K_p' = K_p$ ). As seen from Fig. 5 (b), the measurement noises result in severe chattering in rotational motion of the robot. On the other hand, control signals of the proposed control design have much less measurement noises, due to an effective exploitation of robot's internal damping. Table IV also shows the calculation results. The performance deterioration of typical ADRC is mainly due to the excessive measurement noises in the control signal.

In our experiments, the robot velocity was obtained by Euler's method using the position data of OptiTrack motion capture system. If the differential gain was selected large, noises will be introduced into the control system. Therefore, due to an effective exploitation of the robot's internal damping,

the proposed control design requires much small or even no differential gain  $K_d$ , which makes it an attractive option in practical applications.

Finally, experiments were also conducted to test the cases that the internal damping (i.e.,  $M^{-1}D$ ) is underestimated and overestimated. Experimental results confirmed the discussions in Section IV. The experimental results are omitted here due to page limitation.

## VI. CONCLUSIONS

In this paper, a new ADRC framework has been proposed by effective exploitation of system's internal damping. Specially, the differential feedback gain can be set as quite small or zero. Thus, measurement noises resulting from differential feedback can be greatly reduced. Firstly, the design principles have been derived from analysis of the system's energy balance, resulting in a physically interpretable design. Specifically, the generalized forces of EL systems, i.e., the workless forces, internal damping forces, gravity forces and unknown dynamic forces, are analyzed from the energy dissipation point. Moreover, the exploitation of system's internal damping has been thoroughly discussed, which is of practical significance for application of the proposed design. Finally, experimental tests on an OMR have verified that the proposed framework can achieve superior control performance only using the internal damping, without any differential feedback. However, the typical ADRC requires large differential feedback gain to introduce enough external damping, while heavy measurement noises are introduced.

It has revealed that it is beneficial to selectively compensate the total disturbance, rather than full compensation, by deep analysis of system's physical structure. To the best of the authors' knowledge, this is the first work that the system's internal damping is explicitly exploited and discussed for the ADRC design. Finally, the proposed scheme is not limited

to ADRC design, but can be a general design principle for disturbance observer-based control scheme.

## VII. APPENDIX

### A. Proof of Theorem 1

Consider the following Lyapunov function:

$$V_1 = \frac{1}{2} \mathbf{s}^T \mathbf{s} = \frac{1}{2} s_1^2 + \frac{1}{2} s_2^2 + \frac{1}{2} s_3^2 \geq 0, \quad (29)$$

where  $\mathbf{s} = [s_1 \ s_2 \ s_3]^T$ , and  $s_i$  is one element of  $\mathbf{s}$ ,  $i = 1, 2, 3$ .

The time derivative of (29) is as follows:

$$\dot{V}_1 = \mathbf{s}^T \dot{\mathbf{s}} = s_1 \dot{s}_1 + s_2 \dot{s}_2 + s_3 \dot{s}_3. \quad (30)$$

By dot-multiplying both sides of the reaching law (17) by  $\mathbf{s}$ , it is easy to verify that  $s_1 \dot{s}_1 < 0$ ,  $s_2 \dot{s}_2 < 0$ , and  $s_3 \dot{s}_3 < 0$ ,  $\forall s_i \neq 0, \dot{s}_i \neq 0$ . Therefore, it follows

$$\dot{V}_1 < 0, \quad \forall s_i \neq 0, \dot{s}_i \neq 0. \quad (31)$$

then it can be obtained that  $s_i \rightarrow 0$  as  $t \rightarrow \infty$ .

Combining the expression (31) and the sliding manifold (16), the estimation errors will converge to the sliding surface:

$$\mathbf{s} = \dot{\tilde{\mathbf{e}}} + \mathbf{\Lambda} \tilde{\mathbf{e}} = \mathbf{0}, \quad (32)$$

which means that  $\dot{\tilde{\mathbf{e}}} \rightarrow \mathbf{0}$  and  $\tilde{\mathbf{e}} \rightarrow \mathbf{0}$  as  $t \rightarrow \infty$ . Note that the estimation error  $\tilde{\mathbf{x}}_1$  in the estimation error dynamics (19) is equal to  $\tilde{\mathbf{e}}$ , thus  $\tilde{\mathbf{x}}_1 \rightarrow \mathbf{0}$  and  $\tilde{\mathbf{x}}_1 \rightarrow \mathbf{0}$  as  $t \rightarrow \infty$ .

Substituting  $\mathbf{s} = \mathbf{0}$  and  $\dot{\tilde{\mathbf{x}}}_1 = \mathbf{0}$  into the estimation error dynamics (19), it can be concluded successively that  $\tilde{\mathbf{x}}_2 = \mathbf{0}$ ,  $\tilde{\mathbf{x}}_2$  is bounded,  $\tilde{\mathbf{x}}_3 = \tilde{\mathbf{x}}_2$  is bounded,  $\dot{\tilde{\mathbf{x}}}_3 = \dot{\mathbf{f}}(t)$  is bounded. Specially, if  $\dot{\mathbf{f}}(t) = \mathbf{0}$ , there is  $\tilde{\mathbf{x}}_1 = \tilde{\mathbf{x}}_2 = \tilde{\mathbf{x}}_3 = \mathbf{0}$ .

Therefore, as  $t \rightarrow \infty$ ,  $\mathbf{s} \rightarrow \mathbf{0}$ , then  $\tilde{\mathbf{x}}_1 \rightarrow \mathbf{0}$ ,  $\tilde{\mathbf{x}}_2 \rightarrow \mathbf{0}$ . Also, if  $\dot{\mathbf{f}}(t)$  is bounded, the bounded convergence of  $\tilde{\mathbf{x}}_3$  can be obtained.

### B. Proof of Theorem 2

**Proof.** Solving equation (26),  $\mathbf{E}(t)$  can be expressed as follows:

$$\mathbf{E}(t) = \left( \mathbf{E}(0) + \int_0^t e^{-\int_0^\tau \mathbf{A}_e(\xi) d\xi} \mathbf{A}_x \tilde{\mathbf{x}}_3(\tau) d\tau \right) e^{\int_0^t \mathbf{A}_e(\tau) d\tau}. \quad (33)$$

It can be obtained from the convergence conclusion of sliding mode ESO that:

$$\begin{cases} (\mathbf{A}_x \tilde{\mathbf{x}}_3)_i = 0, & i = 1, 2, 3 \\ |(\mathbf{A}_x \tilde{\mathbf{x}}_3)_i| = |\tilde{\mathbf{x}}_{3(i-3)}| \leq \sigma_{3(i-3)}, & i = 4, 5, 6 \end{cases} \quad (34)$$

where  $\mathbf{A}_x \tilde{\mathbf{x}}_3 \in \mathbb{R}^{6 \times 1}$ , and the  $i$ th element of which is  $(\mathbf{A}_x \tilde{\mathbf{x}}_3)_i$  ( $i = 1, 2, \dots, 6$ ).  $\tilde{\mathbf{x}}_{3j}$  and  $\sigma_{3j}$  represent the  $j$ th element of  $\tilde{\mathbf{x}}_3$  and  $\sigma_3$  respectively.

Define  $\varphi(t) = e^{\int_0^t \mathbf{A}_e(\tau) d\tau} \int_0^t e^{-\int_0^\tau \mathbf{A}_e(\xi) d\xi} \mathbf{A}_x \tilde{\mathbf{x}}_3(\tau) d\tau$ ,  $\mathbf{\Gamma} = \begin{bmatrix} 0 & 0 & 0 & \lambda_1 & \lambda_2 & \lambda_3 \end{bmatrix}^T$ , where  $\lambda_j = \sigma_{3j}$  ( $j = 1, 2, 3$ ). The numerical comparison of the matrices below

represents the numerical comparison between corresponding elements. Then it has

$$\begin{aligned} \varphi(t) &\leq e^{\int_0^t \mathbf{A}_e(\tau) d\tau} \int_0^t e^{-\int_0^\tau \mathbf{A}_e(\xi) d\xi} \mathbf{\Gamma} d\tau \\ &= e^{\mathbf{A}_e t} (-\mathbf{A}_e^{-1} e^{-\mathbf{A}_e t} + \mathbf{A}_e^{-1}) \mathbf{\Gamma}. \end{aligned} \quad (35)$$

The inequation (35) can be further derived as:

$$|\varphi_i(t)| \leq |(\mathbf{A}_e^{-1} \mathbf{\Gamma})_i| + |(\mathbf{A}_e^{-1} e^{\mathbf{A}_e t} \mathbf{\Gamma})_i|, \quad (36)$$

where  $i = 1, 2, \dots, 6$ .

The inverse of matrix  $\mathbf{A}_e$  is

$$\mathbf{A}_e^{-1} = \begin{bmatrix} \mathbf{A}_{e1} & \mathbf{A}_{e2} \\ \mathbf{I}_3 & \mathbf{O}_3 \end{bmatrix}, \quad (37)$$

where

$$\mathbf{A}_{e1} = \begin{bmatrix} -\frac{2\xi}{\omega_c} & 0 & 0 \\ 0 & -\frac{2\xi}{\omega_c} & 0 \\ 0 & 0 & -\frac{2\xi}{\omega_c} \end{bmatrix}, \quad \mathbf{A}_{e2} = \begin{bmatrix} -\frac{1}{\omega_c^2} & 0 & 0 \\ 0 & -\frac{1}{\omega_c^2} & 0 \\ 0 & 0 & -\frac{1}{\omega_c^2} \end{bmatrix}.$$

Then the term  $|(\mathbf{A}_e^{-1} \mathbf{\Gamma})_i|$  is as follows:

$$|(\mathbf{A}_e^{-1} \mathbf{\Gamma})_i| = \begin{cases} \frac{\lambda_i}{\omega_c^2}, & i = 1, 2, 3 \\ 0, & i = 4, 5, 6 \end{cases}. \quad (38)$$

Since  $\mathbf{A}_e$  is Hurwitz, the following inequation is established after a finite time  $T$  when the estimation errors of ESO are bounded:

$$|(e^{\mathbf{A}_e t} \mathbf{\Gamma})_i| \leq \frac{3\lambda_{max}}{\omega_c^k} \quad (i = 1, 2, \dots, 6), \quad (39)$$

where  $\lambda_{max} = \max\{\lambda_1, \lambda_2, \lambda_3\}$  and  $k > 6$ .

Combining (36)-(37), the closed-loop system satisfies:

$$|\varphi_i(t)| \leq \begin{cases} \frac{\lambda_i}{\omega_c^2} + \frac{3\lambda_{max}(2\xi\omega_c+1)}{\omega_c^{k+2}}, & i = 1, 2, 3 \\ \frac{3\lambda_{max}}{\omega_c^k}, & i = 4, 5, 6 \end{cases}. \quad (40)$$

On the other hand,

$$\left| \left( e^{\int_0^t \mathbf{A}_e(\tau) d\tau} \mathbf{E}(0) \right)_i \right| = |(e^{\mathbf{A}_e t} \mathbf{E}(0))_i| \leq \frac{6E_{max}(0)}{\omega_c^k}, \quad (41)$$

where  $E_{max}(0) = \max\{E_i(0)\}$  ( $i = 1, 2, \dots, 6$ ).

Finally, the following conclusion can be obtained:

$$|E_i(t)| \leq \rho_i, \quad (42)$$

where

$$\rho_i = \begin{cases} \frac{6E_{max}(0)}{\omega_c^k} + \frac{\lambda_i}{\omega_c^2} + \frac{3\lambda_{max}(2\xi\omega_c+1)}{\omega_c^{k+2}}, & i = 1, 2, 3 \\ \frac{6E_{max}(0)}{\omega_c^k} + \frac{3\lambda_{max}}{\omega_c^k}, & i = 4, 5, 6 \end{cases}.$$

## REFERENCES

- [1] J. Han, "From PID to active disturbance rejection control," *IEEE transactions on Industrial Electronics*, vol. 56, no. 3, pp. 900–906, 2009.
- [2] C. Ren, X. Li, X. Yang, and S. Ma, "Extended state observer based sliding mode control of an omnidirectional mobile robot with friction compensation," *IEEE Transactions on Industrial Electronics*, vol. 66, no. 12, pp. 9480–9489, 2019.
- [3] X. Hai, Z. Wang, Q. Feng, Y. Ren, B. Xu, J. Cui, and H. Duan, "Mobile robot ADRC with an automatic parameter tuning mechanism via modified pigeon-inspired optimization," *IEEE/ASME Transactions on Mechatronics*, vol. 24, no. 6, pp. 2616–2626, 2019.

- [4] Z. Peng and J. Wang, "Output-feedback path-following control of autonomous underwater vehicles based on an extended state observer and projection neural networks," *IEEE Transactions on Systems, Man, and Cybernetics: Systems*, vol. 48, no. 4, pp. 535–544, 2017.
- [5] Z. Li, I. V. Kolmanovskiy, E. M. Atkins, J. Lu, D. P. Filev, and Y. Bai, "Road disturbance estimation and cloud-aided comfort-based route planning," *IEEE Transactions on Cybernetics*, vol. 47, no. 11, pp. 3879–3891, 2017.
- [6] L. Liu, D. Wang, Z. Peng, T. Li, and C. L. P. Chen, "Cooperative path following ring-networked under-actuated autonomous surface vehicles: Algorithms and experimental results," *IEEE Transactions on Cybernetics*, vol. 50, no. 4, pp. 1519–1529, 2020.
- [7] Y. Huang, J. Wang, D. Shi, J. Wu, and L. Shi, "Event-triggered sampled-data control: An active disturbance rejection approach," *IEEE/ASME Transactions on Mechatronics*, vol. 24, no. 5, pp. 2052–2063, 2019.
- [8] J. Sun, J. Yang, S. Li, and W. X. Zheng, "Sampled-data-based event-triggered active disturbance rejection control for disturbed systems in networked environment," *IEEE Transactions on Cybernetics*, vol. 49, no. 2, pp. 556–566, 2019.
- [9] J. Sun, J. Yang, S. Li, and W. X. Zheng, "Output-based dynamic event-triggered mechanisms for disturbance rejection control of networked nonlinear systems," *IEEE Transactions on Cybernetics*, vol. 50, no. 5, pp. 1978–1988, 2020.
- [10] C. Wang, Z. Zuo, Z. Qi, and Z. Ding, "Predictor-based extended-state-observer design for consensus of MASs with delays and disturbances," *IEEE Transactions on Cybernetics*, vol. 49, no. 4, pp. 1259–1269, 2019.
- [11] F. Alonge, M. Cirrincione, F. D'Ippolito, M. Pucci, and A. Sferlazza, "Robust active disturbance rejection control of induction motor systems based on additional sliding-mode component," *IEEE Transactions on Industrial Electronics*, vol. 64, no. 7, pp. 5608–5621, 2017.
- [12] B. Du, S. Wu, S. Han, and S. Cui, "Application of linear active disturbance rejection controller for sensorless control of internal permanent-magnet synchronous motor," *IEEE Transactions on Industrial Electronics*, vol. 63, no. 5, pp. 3019–3027, 2016.
- [13] M. Ye and G. Hu, "Solving potential games with dynamical constraint," *IEEE Transactions on Cybernetics*, vol. 46, no. 5, pp. 1156–1164, 2016.
- [14] B. Guo and Z. Zhao, *Active Disturbance Rejection Control for Nonlinear Systems: An Introduction*. Singapore; Hoboken, NJ: John Wiley & Sons, 2016.
- [15] H. Sira-Ramírez, A. Luviano-Juárez, M. Ramírez-Neira, and E. W. Zurita-Bustamante, *Active Disturbance Rejection Control of Dynamic Systems*. Elsevier, 2017.
- [16] J. Y. Lau, W. Liang, and K. K. Tan, "Motion control for piezoelectric-actuator-based surgical device using neural network and extended state observer," *IEEE Transactions on Industrial Electronics*, vol. 67, no. 1, pp. 402–412, 2019.
- [17] Y. Yuan, Y. Yu, and L. Guo, "Nonlinear active disturbance rejection control for the pneumatic muscle actuators with discrete-time measurements," *IEEE Transactions on Industrial Electronics*, vol. 66, no. 3, pp. 2044–2053, 2018.
- [18] M. R. Mokhtari, A. C. Braham, and B. Cherki, "Extended state observer based control for coaxial-rotor UAV," *ISA Transactions*, vol. 61, pp. 1–14, 2016.
- [19] H. Yang, X. Fan, P. Shi, and C. Hua, "Nonlinear control for tracking and obstacle avoidance of a wheeled mobile robot with nonholonomic constraint," *IEEE Transactions on Control Systems Technology*, vol. 24, no. 2, pp. 741–746, 2015.
- [20] S. Lin and B. Li, "Shift force optimization and trajectory tracking control for a novel gearshift system equipped with electromagnetic linear actuators," *IEEE/ASME Transactions on Mechatronics*, vol. 24, no. 4, pp. 1640–1650, 2019.
- [21] N. Gu, Z. Peng, D. Wang, Y. Shi, and T. Wang, "Antidisturbance coordinated path following control of robotic autonomous surface vehicles: Theory and experiment," *IEEE/ASME Transactions on Mechatronics*, vol. 24, no. 5, pp. 2386–2396, 2019.
- [22] B. Ahi and M. Haeri, "Linear active disturbance rejection control from the practical aspects," *IEEE/ASME Transactions on Mechatronics*, vol. 23, no. 6, pp. 2909–2919, 2018.
- [23] Z. Chu, Y. Sun, C. Wu, and N. Sepahri, "Active disturbance rejection control applied to automated steering for lane keeping in autonomous vehicles," *Control Engineering Practice*, vol. 74, pp. 13–21, 2018.
- [24] H. Yang, Y. Xu, Y. Xia, and J. Zhang, "Networked predictive control for nonlinear systems with arbitrary region quantizers," *IEEE Transactions on Cybernetics*, vol. 47, no. 8, pp. 2244–2255, 2017.
- [25] K. Meng, H. Yang, Y. Wang, and D. Sun, "Modeling and control of single-cell migration induced by a chemoattractant-loaded microbead," *IEEE Transactions on Cybernetics*, vol. 49, no. 2, pp. 427–439, 2019.
- [26] J. Sun, Z. Pu, and J. Yi, "Conditional disturbance negation based active disturbance rejection control for hypersonic vehicles," *Control Engineering Practice*, vol. 84, pp. 159–171, 2019.
- [27] J. Yao and W. Deng, "Active disturbance rejection adaptive control of hydraulic servo systems," *IEEE Transactions on Industrial Electronics*, vol. 64, no. 10, pp. 8023–8032, 2017.
- [28] J. Yao, Z. Jiao, and D. Ma, "Adaptive robust control of dc motors with extended state observer," *IEEE Transactions on Industrial Electronics*, vol. 61, no. 7, pp. 3630–3637, 2013.
- [29] X. Shao, N. Liu, J. Liu, and H. Wang, "Model-assisted extended state observer and dynamic surface control based trajectory tracking for quadrotors via output feedback mechanism," *International Journal of Robust & Nonlinear Control*, vol. 28, no. 1, pp. 2404–2423, 2017.
- [30] R. Ortega, A. Loria, P. Nicklasson, and H. Sira-Ramírez, *Passivity-based control of Euler-Lagrange systems: mechanical, electrical and electromechanical applications*. London, U.K.: Springer, 1998.
- [31] C. Ren, Y. Ding, and S. Ma, "Passivity-based active disturbance rejection control of an omnidirectional mobile robot," in *Proceedings of IEEE 8th Annual International Conference on CYBER Technology in Automation, Control, and Intelligent Systems (CYBER)*, (Tianjin, China), pp. 1513–1518, Jul. 2018.
- [32] C. Ren, Y. Ding, S. Ma, L. Hu, and X. Zhu, "Passivity-based tracking control of an omnidirectional mobile robot using only one geometrical parameter," *Control Engineering Practice*, vol. 90, pp. 160–168, 2019.
- [33] Z. Gao, "Active disturbance rejection control: a paradigm shift in feedback control system design," in *Proceedings of 2006 American control conference*, (Minneapolis, MN, USA), pp. 2399–2405, Jul. 2006.
- [34] O. Tutsoy, D. E. Barkana, and H. Tugal, "Design of a completely model free adaptive control in the presence of parametric, non-parametric uncertainties and random control signal delay," *ISA Transactions*, vol. 76, pp. 67–77, 2018.
- [35] O. Tutsoy and S. Colak, "Adaptive estimator design for unstable output error systems: A test problem and traditional system identification based analysis," *Proceedings of the Institution of Mechanical Engineers Part I Journal of Systems & Control Engineering*, vol. 229, no. 10, pp. 902–916, 2015.
- [36] C. Ren and S. Ma, "Dynamic modeling and analysis of an omnidirectional mobile robot," in *Proceedings of 2013 IEEE/RSJ International Conference on Intelligent Robots and Systems*, (Tokyo, Japan), pp. 4860–4865, Nov. 2013.
- [37] R. Madoński and P. Herman, "Survey on methods of increasing the efficiency of extended state disturbance observers," *ISA Transactions*, vol. 56, pp. 18–27, 2015.
- [38] Z. Gao, "Scaling and bandwidth-parameterization based controller tuning," in *Proceedings of the American control conference*, (Minnesota, USA), pp. 4989–4996, Jun. 2003.
- [39] J. Li, Y. Xia, X. Qi, and Z. Gao, "On the necessity, scheme and basis of the linear-nonlinear switching in active disturbance rejection control," *IEEE Transactions on Industrial Electronics*, vol. 64, no. 2, pp. 1425–1435, 2017.

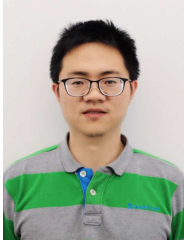


**Chao Ren** was born in Shandong Province, China, 1986. He received the B.Eng. degree in electrical engineering and automation from Shandong Jianzhu University (Jinan, China) in 2009, and the M.S. degree in control science and control engineering from Harbin Institute of Technology (Harbin, China) in 2011. He received his Ph.D. degree in Robotics from Ritsumeikan University (Kyoto, Japan) in 2015. He is currently an Assistant Professor in Tianjin University, Tianjin, China. His research interests

include robot design and control.



**Yutong Ding** was born in Hebei Province, China, 1996. She received the bachelor of engineering degree in Automation from School of Electrical and Information Engineering, Tianjin University, Tianjin, China, in 2018. She is currently a graduate student at the School of Electrical and Information Engineering, Tianjin University, Tianjin, China, working toward the master's degree in Control Science and Engineering. Her current research interests include robot control.



**Liang Hu** received both the B.E. and M.E. degrees from Harbin Institute of Technology, China, in 2008 and 2010, respectively, and the Ph.D. degree from Brunel University London, U.K., in 2016. Dr Hu is a lecturer in the School of Computer Science and Electronic Engineering, University of Essex, UK. Prior to that, he was a Lecturer with the School of Computer Science and Informatics, De Montfort University, UK. He did the postdoctoral research at Queen's University Belfast and Loughborough University from 2016

to 2018. His research interests include Bayesian signal processing, planning and control and their applications in autonomous systems and intelligent transport systems.



**Zhaojie Ju** received the B.S. in automatic control and the M.S. in intelligent robotics both from Huazhong University of Science and Technology, China, and the Ph.D. degree in intelligent robotics at the University of Portsmouth, UK. He held a research appointment at the University College London, London, U.K., before he started his independent academic position at the University of Portsmouth, U.K., in 2012. His research interests include machine intelligence, pattern recognition, and robot control. He has authored

or co-authored over 170 publications in journals, book chapters, and conference proceedings and received four best paper awards and one Best AE Award in ICRA2018. Dr. Ju is an Associate Editor of the IEEE Transactions on Cybernetics, Journal of Intelligent & Fuzzy Systems, and International Journal of Fuzzy Systems.



**Jinguo Liu** received his Ph.D. degree in mechatronics from Shenyang Institute of Automation (SIA), Chinese Academy of Sciences (CAS) in 2007. Since January 2011, he has been a Full Professor with SIA, CAS. In addition, he has held the Assistant Director position of State Key Laboratory of Robotics since 2008 and the Associate Director position of Center for Space Automation Technologies and Systems since 2015. His research interests include design and control of bio-inspired robotics and space robotics. He

has authored/coauthored four books, over one hundred papers and fifty patents in these areas. Dr. Liu services as an Editor of several journals such as IEEE Transaction on Mechatronics, IEEE Access, Mechanical Sciences, and Chinese Journal of Mechanical Engineering.



**Shugen Ma** received his Ph.D. degree in Mechanical Engineering Science from Tokyo Institute of Technology (Tokyo, Japan) in 1991. Since July 1993 he has been with Ibaraki University (Japan) as an Assistant Professor of Department of Systems Engineering. In October 2005, he joined Ritsumeikan University and currently is a professor in the Department of Robotics. He is also holding professor position at Tianjin University.

His current research interests include the design and control of new types of robots, rescue robotics, and Biorobotics. He is a fellow of the IEEE and JSME. He was an Associate Editor of the IEEE Transaction on Robotics from December 2003 to November 2007, an Editor of Advanced Robotics from April 2007, and serves many societies and conferences including the general chair of ROBIO 2004, ROBIO 2010 and ROBIO 2016.